Geomechanics and Engineering, *Vol. 42, No. 1 (2025) 1-14*
https://doi.org/10.12989/gae.2025.42.1.001

Study on the effect of blasting breaking rock under different stemming condition

Nan Yao[1,2a], Cheng Tan[1b], Yufei Li*[1,2], Felix Oppong[1c], Wei Jiang[3d] and Kunfeng Lin[4e]

[1]*School of Resources and Environmental Engineering, Wuhan University of Science and Technology, Wuhan 430081, China*
[2]*Hubei Key Laboratory for Efficient Utilization and Agglomeration of Metallurgic Mineral Resource, Hubei, Wuhan 430081, China*
[3]*Baosteel Resources Group Co, Shanghai 201800, China*
[4]*Wuhan Safety and Environmental Protection Research Institute of Sinosteel Group Co, Wuhan 430081, China*

(*Received August 16, 2023, Revised May 22, 2025, Accepted June 12, 2025*)

Abstract. To study the blasting and rock-breaking effects of stemming materials and their mechanisms, the friction force tests on various stemming materials were conducted as well as field experiments involving blasting of concrete specimens under different stemming conditions. The internal blasting stress and fragmentation of the specimens after blasting were analyzed, and further discussions on rock blasting damage were conducted through numerical simulations. The results revealed that when stemming materials were used, the internal blasting stress within the rock was higher, and the size of rock fragments after blasting was smaller. Moreover, under stemming conditions, the distribution range of internal blasting stress widened, the stress peak increased, and the extent of rock damage and fragmentation area increased. The sealing performance of stemming materials was closely linked to their frictional resistance and sealing capability. Among the materials studied, polyurethane foam material demonstrated superior stemming effectiveness and convenient usage, making it a promising choice for engineering applications. These research findings provide valuable guidance for blasthole stemming in rock blasting scenarios.

Keywords: blasting stress; friction; numerical simulation; rock blasting; rock size; stemming material

1. Introduction

Currently, borehole blasting technique is mainly used in underground geotechnical engineering (Chen *et al*. 2021a, Li *et al*. 2009, Konya and Walter 2003), and the stemming of blastholes has become an important practice in the construction process. Previous studies have highlighted the significance of stemming during blasting. Firstly, stemming facilitates the complete reaction of explosives within the blasthole, extending the duration of explosive gas action in the rock (José *et al*. 2007, Cevizci and Ozkahraman 2012, Onder *et al*. 2007, Lee *et al*. 2009, Otuonye *et al*. 1983, Choudhary and Rai 2013, Sazid *et al*. 2012). Secondly, it increases the effective stress of shock waves, enhancing the breaking of rock and improving the blasting effectiveness, which ultimately reduces blasting costs (Sazid *et al*. 2012, Dally *et al*. 1975, Kojovic 2005). Lastly, stemming effectively reduces blast punching and enhances blast safety (Kojovic 2005, Zhang *et al*. 2020, Fourney *et al*. 1981, Brinkmann 1990). However, it is common for workers in underground mining, tunnel excavation, and other underground construction projects to neglect stemming the blastholes after loading explosives. This is primarily attributed to the tedious nature of stemming operation and the desire to streamline operations and save time. While some projects employ traditional stemming materials like clay and mud, their effectiveness in rock fragmentation is unsatisfactory. Currently, on-site stemming materials such as expanding agents include polyurethane foam agents. Additionally, materials like steel molds and plastic molds are also utilized. The reasons behind the contrasting effects of various stemming materials on rock fragmentation during blasting remain unclear. Hence, it is essential to conduct comprehensive research to understand the action mechanism and evaluate the blasting and rock-breaking effects under different stemming conditions.

Several researchers have conducted relevant research on the effectiveness of various stemming materials. Ma *et al*. (2020) introduced a novel stemming method that combines the use of mud stemming and expanding foam materials. The results indicated that this method offers several advantages over traditional stemming methods. These include enhanced stemming effectiveness, reduced specific consumption of explosives, and increased blast penetration. Chen *et al*. (2021b) conducted a theoretical analysis of the force mechanism involved in stemming. Subsequently, they proposed a time-sharing piecewise solution method for

*Corresponding author, Lecturer
E-mail: liyufei@wust.edu.cn
[a]Associate Professor
E-mail: yaonan@wust.edu.cn
[b]M. Sc. Student
E-mail: 923014867@qq.com
[c]M. Sc. Student
E-mail: fe.oppong@gmail.com
[d]Senior engineer
E-mail: 279079840@qq.com
[e]Senior engineer
E-mail: 353782831@qq.com

ISSN: 2005-307X (Print), 2092-6219 (Online)

modeling the movement process of the stemming structure using the time-space discretization approach. The results demonstrated that factors such as explosion load, duration of detonation gas, sliding friction coefficients, borehole diameters, and stemming length significantly affect the movement of the stemming structure. Furthermore, the reliability of the proposed method has been preliminarily verified through field applications. Zhang *et al*. (2021) conducted blasting experiments on cylindrical granite specimens under different stemming conditions. They discovered that, at a specific charge-to-mass ratio, fully sand-stemmed blasting yielded better fragmentation compared to partially steel-stemmed blasting. The partially steel-stemmed blasting led to earlier gas jetting at the neck of the blasthole in comparison to fully sand-stemmed blasting. Liu *et al*. (2015) conducted a feasibility analysis and model experiment on the application of mud-based stemming material. The results demonstrated that the composite filling structure comprising mud-based stemming material and river sand effectively resolved the stemming issue. Yan *et al*. (2014) implemented a water-soil composite stemming method in tunnel excavation. They observed that a significant higher blasthole pressure generated during blasting compared to pure clay stemming. This finding was further confirmed through practical engineering examples. Liu *et al*. (2021) utilized ANSYS/LS-DYNA software to analyze the effects of different initiation methods and stemming materials on rock drilling. The results indicated that clay and water-based stemming methods resulted in more uniform stress disturbance and prolonged stress duration during initiation, ultimately leading to improved overall blasting effects.

Previous literature primarily focused on analyzing the blasting effects of one or two types of stemming materials. Building upon the achievements of the aforementioned scholars, this paper aims to further investigate this topic. In this study, four different stemming materials, namely clay, polyurethane foam agent, steel mold, and plastic mold, were selected for examination. Additionally, a control group without stemming was included for comparison. The blasting rock-breaking effects of these materials were thoroughly analyzed and compared. The study reveals that (Chen *et al*. 2021b, Zong 1996, Luo and Shen 2006), with consistent stemming length as a condition, the main factor influencing the effectiveness of stemming was the frictional resistance between the stemming material and the blasthole wall. Therefore, the first step involved testing the frictional forces of the various stemming materials. Secondly, field blasting experiments were conducted on concrete specimens filled with cement mortar under different stemming conditions. The blasting effectiveness was evaluated by considering the effective stress (José *et al*. 2007, Cevizci and Ozkahraman 2012, Onder *et al*. 2007, Lee *et al*. 2009, Otuonye *et al*. 1983) for rock breaking and the degree of specimen fragmentation (Zhang *et al*. 2021). In the third phase, finite element numerical simulations were performed using ANSYS/LS-DYNA software to compare the effectiveness of stemming under different stemming conditions. Stress nephogram, stress-time curves, and damage nephogram were analyzed to evaluate the stemming effects. The results of the numerical simulations were then compared with the findings from the field blasting experiments. Finally, the action mechanisms for different stemming materials were discussed

2. Experiments

2.1 Friction experiment

The frictional forces of the four different types of stemming materials were tested using the pull-out method. These materials included clay, polyurethane foam agent, steel mold, and plastic mold. The anchor rod pull-out tester was used to measure the frictional forces. Fig. 1 shows the stemming materials and the testing method. To conduct the tests, concrete was poured into a 300 mm*200 mm iron mold, leaving a mock blasthole with a diameter of 40 mm and a depth of 100 mm. For the steel mold and plastic mold, steel bars were welded onto the upper part. They were inserted into the blasthole and subsequently pulled out. As for the polyurethane foam material, it was poured into the blasthole and allowed to cure, after which a homemade steel bar was used to extract it. The same approach was employed to test the clay. The measurement results can be observed in Fig. 2.

Based on the observations in Fig. 2, the ranking of frictional resistance generated by different stemming materials on the blasthole wall can be summarized as follows: steel mold > plastic mold ≈ polyurethane foam agent > clay. The steel mold exhibited the highest frictional resistance because its outer casing fastened into the blasthole wall. In contrast, the plastic mold was inserted as a whole into the blasthole, resulting in significant frictional resistance for both materials. Clay, being a loose material, exhibited relatively low frictional resistance against the blasthole wall. On the other hand, the polyurethane foam material formed a solid seal, completely filling the blasthole's cross-section. It adhered firmly to the blasthole wall, and the frictional resistance it generated against external forces originated from the bonding force between the material and the blasthole wall (Xu *et al*. 2023, Wang *et al*. 2023). The adhesive ability of the polyurethane foam material allowed it to generate substantial frictional resistance when subjected to external pushing forces. This, in turn, greatly enhanced the frictional force between the material and the blasthole wall, thereby imposing strong constraints on their relative movement.

2.2 Blasting experiment

2.2.1 Experimental method

The blasting experiment was conducted in 5 groups, with each group consisting of 3 specimens, resulting in a total of 15 cement mortar concrete experiment specimens. The dimensions of these specimens are 400 mm*400 mm*400 mm, and they included a reserved central blasthole. The blasthole had a depth of 200 mm and a diameter of 40 mm. The mechanical parameters of the specimens, obtained through indoor testing, are presented in

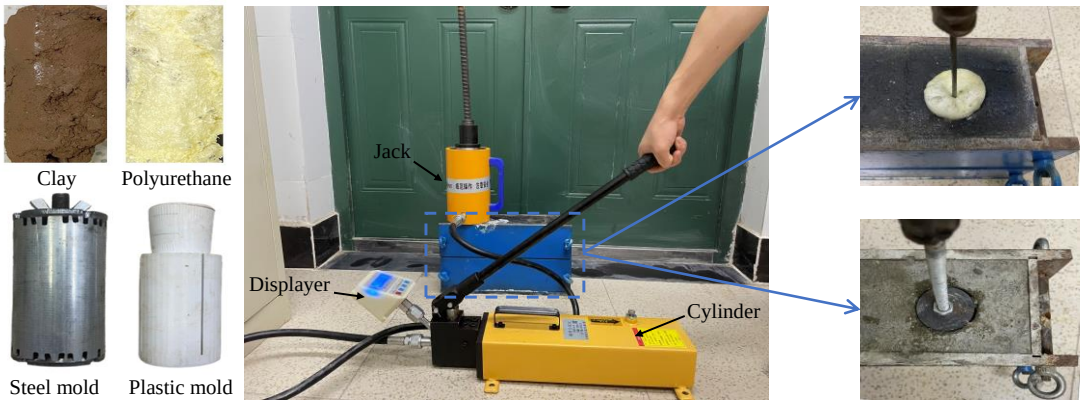

Fig. 1 Stemming materials and testing method

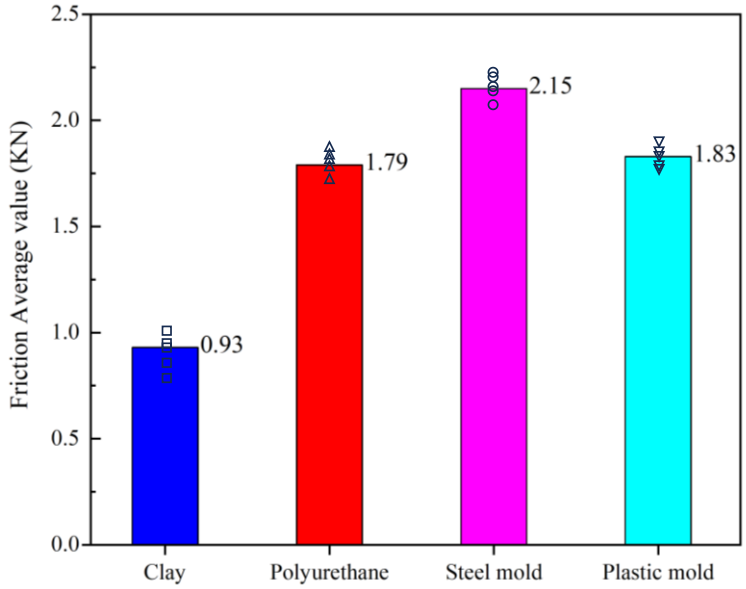

Fig. 2 Frictional forces of different stemming materials

Table 1 Mechanical parameters of the concrete experiment specimens

parameters	value	parameters	value
specimen density ρ (kg/m^3)	2.1	young's modulus E (MPa)	316
uniaxial compressive strength σ_c (MPa)	15.8	poisson's ratio μ	0.25
tensile strength σ_t (MPa)	1.5	internal friction angle φ (°)	31

Table 1. Prior to pouring, strain bricks with the same material composition as the specimens were prepared in advance. Strain gauges were attached to these strain bricks. Each specimen contained two strain bricks embedded at distances of 50 mm and 100 mm from the blasting center, respectively. The initiation of the experiment employed electronic detonators, and 2nd grade emulsion explosives were chosen for charging. Each concrete experiment specimen required 50 g of explosives, measured using an electronic scale, with a charging length of approximately 50mm. The length of stemming was consistent for each group, set at 100mm. The blasting experiment equipment and procedure can be seen in Fig. 3.

The first group of experiment specimens remained unstemmed, while the remaining four groups utilized four different stemming materials. For specimens stemmed with clay and polyurethane foam material, a curing period of approximately 15 minutes was allowed prior to the blasting operation. In the case of the steel mold and plastic mold, there was a gap of approximately 5 mm on one side between the molds and the blasthole wall. This gap served as a pathway for the detonator wires, and the molds were securely fastened before the blasting operation. The experimental requirements are shown in Table 2.

2.2.2 Rock fragmentation results

The fragmented rocks resulting from the explosion were

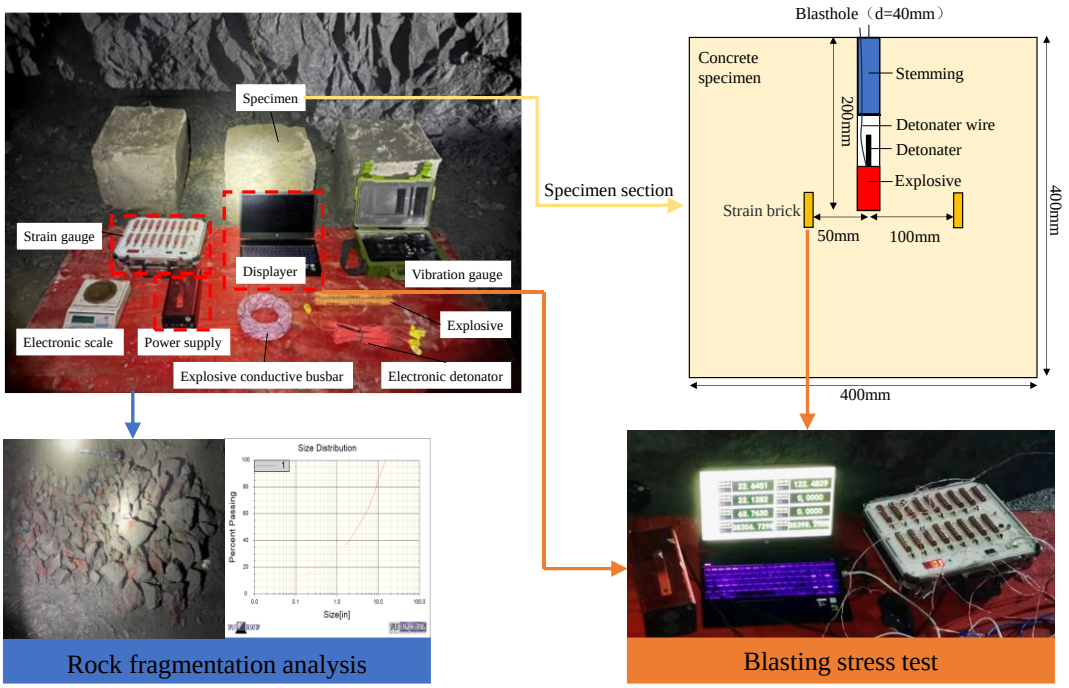

Fig. 3 Blasting experiment

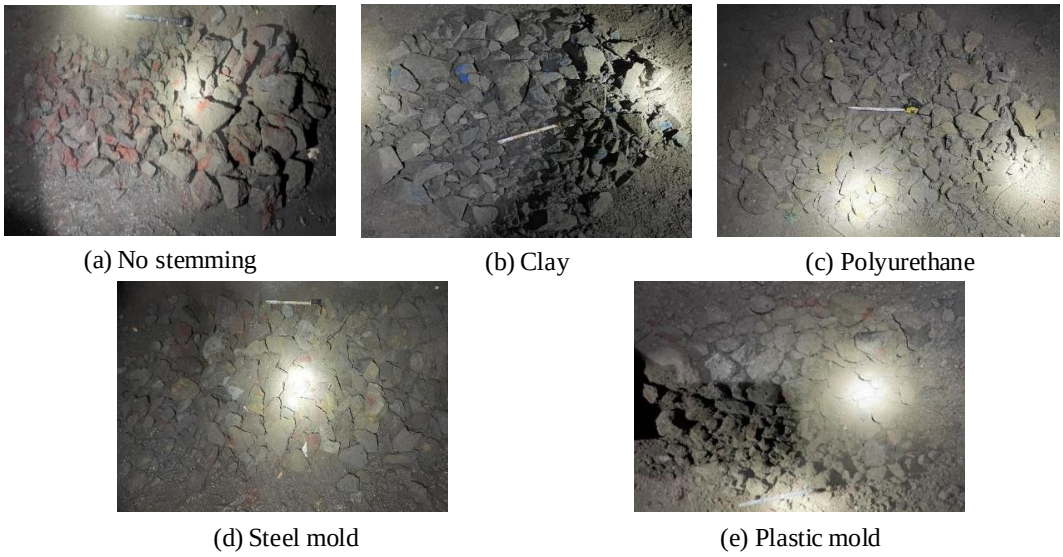

(a) No stemming (b) Clay (c) Polyurethane

(d) Steel mold (e) Plastic mold

Fig. 4 Exploded pile diagram of all experiment specimens

Table 2 Experimental requirements

Stemming materials	Control group	Clay	Polyurethane foam agent	Steel mold	Plastic mold
Experimental requirements	Remained unstemmed	Curing period of approximately 15 minutes was allowed prior to the blasting operation		Gap of approximately 5mm on one side between the molds and the blasthole wall	

collected and arranged in an organized manner. To calibrate the actual size of the rocks in the photos, a 300 mm measuring tape was placed within the blast pile as a reference object, as shown in Fig. 4. It is evident that all the experiment specimen models were completely destroyed, resulting in irregularly shaped fragments of varying sizes. The longest fragment measured reached a length of 281 mm. Following the photo documentation, the Split-Desktop software, which utilizes image processing technology, can be employed to analyze the rock fragmentation and accurately determine the sizes of the fragments.

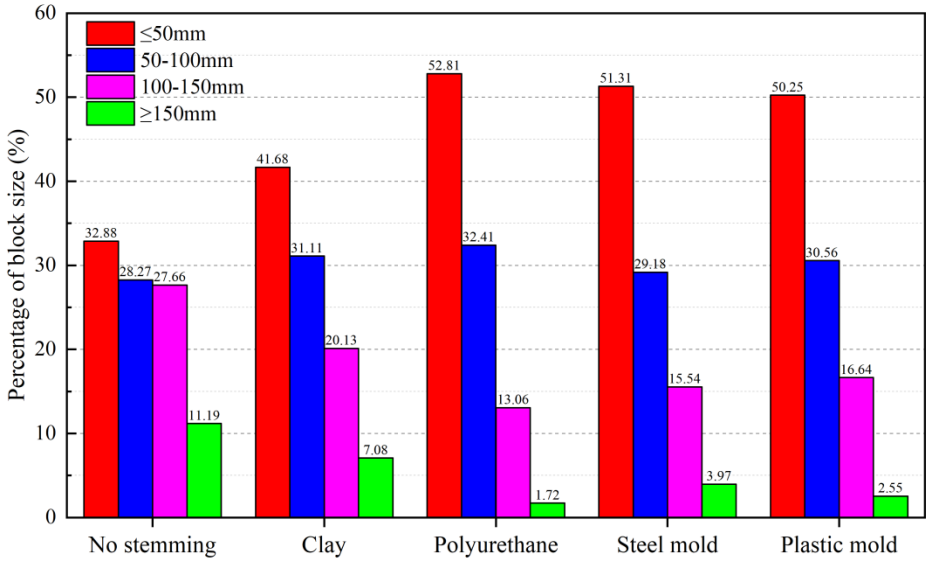

Fig. 5 Rock size statistics graph

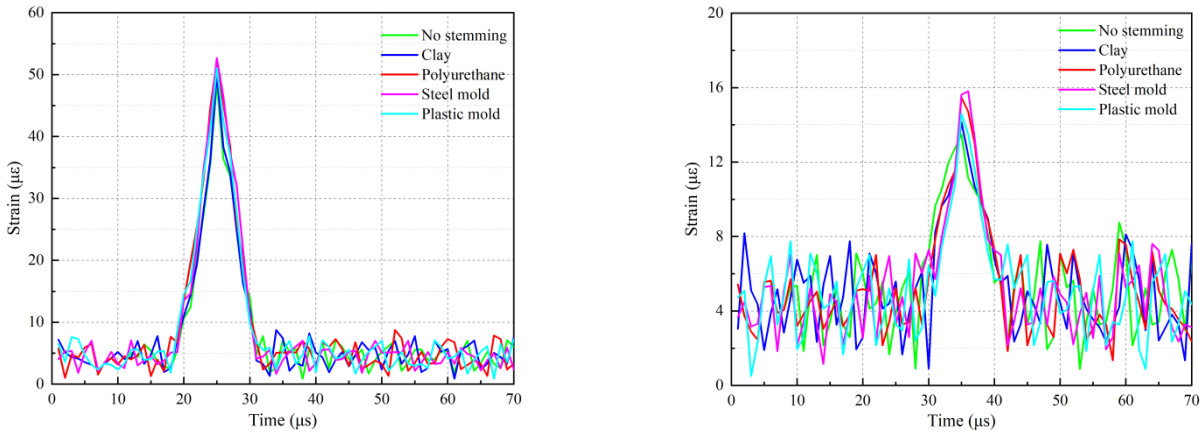

(a) 50 mm from the blast center (b) 100 mm from the blast center

Fig. 6 Typical dynamic strain-time curves of blasting under different stemming conditions

Therefore, the Split-Desktop software was used to analyze the size of the rocks following the explosion. The process involved importing the images into the system and annotating the actual size of the reference object.

Subsequently, the edges of the rocks were delineated (Xie *et al*. 2021). Using the algorithms within the Split-Desktop software, the analysis entailed examining the sizes of rocks at various levels and determining the proportion of different sizes within the blast pile under different stemming conditions, as shown in Fig. 5.

Based on the fragmentation size statistics above, noticeable differences in fragment size were evident following blasting under different stemming conditions. Among them, the unstemmed group showed larger average fragment sizes, with over 60% of the fragments measuring above 50 mm, and more than 10% exceeding 150 mm in size. Clay material stemming also resulted in over 50% of the fragments exceeding 50 mm in size. In contrast, the polyurethane foam material, steel mold, and plastic mold stemming yielded smaller fragment sizes, with the majority of fragments measuring below 50mm. The overall distribution of fragment sizes for these three materials showed relatively minor variations. By employing stemming within the blasthole, the energy generated by the explosives was more effectively utilized for rock fragmentation, thereby reducing the occurrence of larger rock fragments.

2.2.3 Blasting stress results

By capturing and processing waveform data, typical dynamic strain-time curves for blasting under different stemming conditions were obtained. These curves are shown in Fig. 6.

Based on Fig. 6, it is evident that the peak strain at a distance of 50mm from the blasting center was notably higher compared to the strain at 100mm. This observation suggests that as the location gets closer to the center of the blasting source, the stress generated during the explosion increased, leading to greater resulting strain.

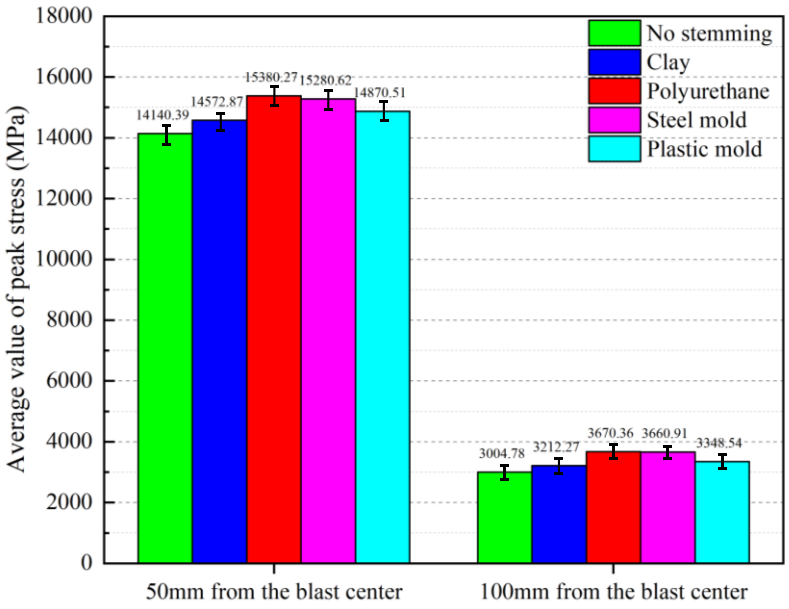

Fig. 7 Peak stress

According to Hooke's Law (Yuan *et al*. 2022), the stress applied to an object is directly proportional to the strain it produces, within the elastic limit. This relationship can be expressed by the Young's modulus, as shown in Eq. (1). The peak stress at each measurement point was calculated using formula in Eq. (2).

$$E = \frac{F_{\Delta} / A}{\Delta L / L_0} \tag{1}$$

Where F_{Δ} represents compressive or tensile force; A represents cross-sectional area or the cross-section perpendicular to the applied force; ΔL represents the change in length (negative for compression, positive for tension); L_0 represents the original length.

$$\sigma = E\varepsilon \tag{2}$$

Where σ represents stress; E represents Young's modulus; and ε represents strain. By using equation (1) and (2), stress can be calculated based on strain. Given that Young's modulus is known, the average values of the peak stresses can be obtained as shown in Fig. 7.

From the graph above, it is evident that the stress exerted on the rock increased as the distance to the blast center decreased. Conversely, as the distance from the blast center increased, the stress decreased significantly. Due to the substantial energy generated during the explosion, the variations in internal blasting stress within the rock under different stemming conditions were relatively minor, ranging from several hundred to one thousand MPa. When polyurethane foam material, steel mold, and plastic mold were used for stemming, the internal blasting stress within the rock was higher. Clay material for stemming followed, and the stress was the lowest when no stemming was used. Stemming enhanced the effective stress of the explosive shock wave for rock fragmentation, rendering the rock more susceptible to crushing and fragmentation.

3. Numerical simulation

3.1 Numerical modeling

The ANSYS/LS-DYNA software was used to established a numerical model that corresponded to the blasting experiment. Through numerical simulations, a comparative analysis of the stemming effects under different conditions was conducted, and the results were compared with the actual blasting experiment. To simplify the calculations and capitalize on the model's symmetry, a numerical model of the blasting finite element was constructed with a 1/4 size, centered on the blasthole. The model comprised four components: rock, explosive, stemming, and air. It has dimensions of 200 mm in length and width, with a height of 400mm. The blasthole measured 200 mm in depth and 40mm in diameter. The charging length was 50mm, while the stemming length was 100 mm. The symmetry plane of the model was constrained using the displacement phase-shift constraint. The upper part of the model was designated as a free surface, while the other surfaces was set as boundaries with non-reflective boundary conditions (LSTC 2003, Li *et al*. 2023a, Xu *et al*. 2021, Wang *et al*. 2021a). The model was meshed using SOLID164 solid elements. The fluid-structure coupling algorithm was applied, utilizing ALE (Arbitrary Lagrangian-Eulerian) elements for air, explosive, and stemming, while Lagrange elements was used for the rock. The parameter units were set to cm-g-μs. The blasting time was set as 100 μs, with an output time interval of 1μs. The blasting initiation point was positioned at the bottom of the blasthole. For visualization purposes, Fig. 8 shows the numerical model and its meshing.

3.2 Parameter selection

3.2.1 Parameters of the rock material

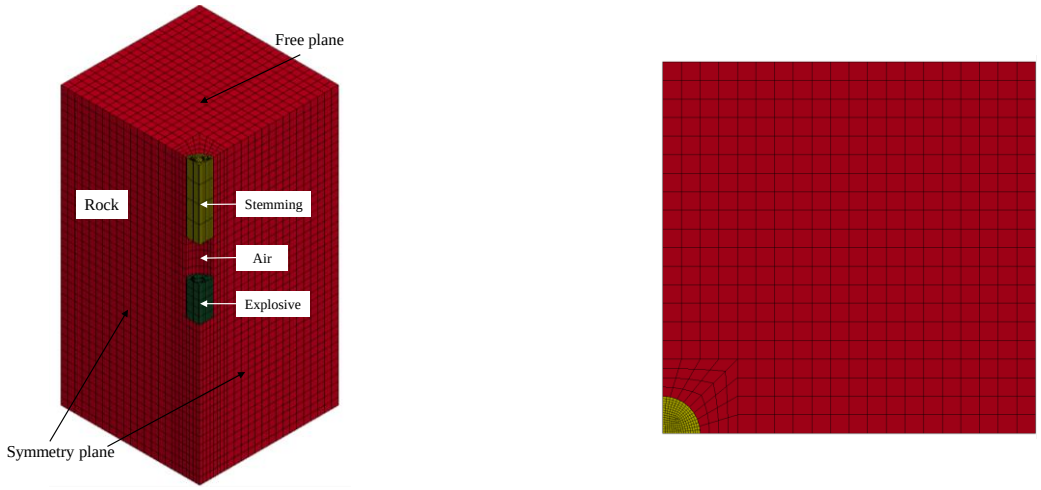

(a) Holistic model (b) Mesh generation

Fig. 8 numerical model and its meshing

Table 3 Parameters for the explosive material and equation of state parameters

parameters	value	parameters	value
explosive density ρ_e (kg/m^3)	1.2	material constant $R1$	5.2
detonation velocity V (m/s)	5200	material constant $R2$	2.1
chapman-Jouguet pressure P (GPa)	21	material constant ω (GPa)	0.5
material constant A (GPa)	485.2	initial internal energy E_i (GPa)	4.12
material constant B (GPa)	6.4		

Table 4 Parameters for the air material and equation of state parameters

parameters	value	parameters	value
air density ρ (kg/m^3)	1.29×10^{-5}	material constant C_4	0.4
material constant C_0	0	material constant C_5	0.4
material constant C_1	0	material constant C_6	0
material constant C_2	0	initial internal energy E (GPa)	0.025
material constant C_3	0		

The rock material parameters were chosen based on the RHT material parameters (Tu and Lu 2010). This material model encompassed compression and tensile failure, strain rate effects, strain hardening, and stress softening phenomena of the material. It provided a comprehensive representation of the dynamic mechanical behavior of brittle materials under various stress states, making it particularly suitable for simulating rock blasting and other nonlinear dynamic impact problems involving significant deformations and high strain rates. The rock parameters are listed in Table 1.

3.2.2 Equation of state and parameters for the explosive material

The calculation model for the explosive material was *MAT_HIGH_EXPLOSIVE_BURN, which utilized the *EOS_JWL equation of state to represent the correlation between volume and pressure of the explosion products following detonation (Mackerle 1999, Wang *et al*. 2021b).

The JWL equation is represented as follows

$$P = A\left[1-\frac{\omega}{R_1V}\right]e^{-R_1V} + B\left[1-\frac{\omega}{R_2V}\right]e^{-R_2V} + \frac{\omega E_0}{V} \tag{3}$$

Where P represents the pressure of the explosion products; V represents the relative volume of the explosion products; E_0 represents the initial specific internal energy of the explosion products; A, B, R_1, and R_2 are material parameters.

The parameters for the explosive material and the equation of state parameters can be found in Table 3.

3.2.3 Parameters for the air material

The calculation model for the air material was *MAT_NULL, and the *EOS_LINEAR_POLYNOMIAL equation of state was used to define the air model. The equation of state is as follows

$$P = C_0 + C_1\mu + C_2\mu^2 + C_3\mu^3 + (C_4 + C_5\mu + C_6\mu^2) \tag{4}$$

Table 5 Clay material parameter

parameters	value	parameters	value
clay density ρ (kg/m^3)	1.8	poisson's ratio μ	0.33
Tangent modulus E_c (MPa)	0.13	yield strength σ_s (MPa)	0.77
elasticity modulus E (MPa)	1.38	internal friction angle φ (°)	30

Table 6 Polyurethane foam material parameter

parameters	value	parameters	value
polyurethane density ρ (kg/m^3)	1.9	poisson's ratio μ	0.35
Cohesion c (MPa)	0.018	yield strength σ_s (MPa)	0.92
elasticity modulus E (MPa)	17	internal friction angle φ (°)	40

Where C_i represents the parameters of the equation of state; E represents the initial specific internal energy per unit relative volume; V represents the relative volume.

The parameters for the air material and the equation of state parameters can be found in Table 4.

3.2.4 Parameters for the stemming material

The material parameters for the stemming unit were defined based on the findings derived from the indoor testing. The maximum frictional force between the stemming unit and the blasthole wall was based on the results obtained from the pull-out experiment. To ensure the parameter coherence in numerical simulation, we conducted numerical simulations using three scenarios: no stemming, clay stemming, and polyurethane foam stemming.

For the clay material, the *MAT_PLASTIC_KINGEMATIC elastoplastic model was used, with its corresponding material parameters presented in Table 5.

The polyurethane foam material was modeled using the SOIL AND FOAM material model, which was suitable for simulating expanding foam materials. The material parameters for this model are shown in Table 6.

3.3.1 Model stress analysis

To study the propagation characteristics of the stress waves in rocks under the different stemming conditions, stress nephogram of rock specimens was extracted at different time intervals, as shown in Fig. 9. The stress nephogram, from left to right, corresponded to time intervals of 30 μs, 40 μs, 50 μs, and 100 μs.

Based on the stress nephogram, it is apparent that during the initial stage of the explosion, stress waves propagated in an arc-shaped waveform from the bottom of the blasthole. Subsequently, they rapidly spread in a fan-shaped pattern towards the surrounding areas. As the shock wave propagated, rocks in proximity to the explosive experience rapid destruction, resulting in the formation of a fractured zone near the blasthole. The combination of the wedging effect of the stress wave and the explosive gases generated tensile stress within the rocks, leading to their tensile failure. As time progressed, the stress wave continued to propagate. However, due to the stemming effect, the stress wave experienced deformation and was accompanied by stress concentration phenomena. This results in the formation of strengthened stress wave zones on both sides of the blasthole, ultimately enhanced the fragmentation of the rocks. In the later stage of the explosion, the rocks in the upper part of the model had already undergone fragmentation, while the residual stress continued to affected the rocks at the bottom of the model. It was evident that due to the stemming effect, the stress wave showed a broader impact range at the bottom of the model, resulting in stronger damage to the rocks in that area. When comparing clay and polyurethane foam materials, it was observed that the use of polyurethane foam material for stemming led to a stress wave with a wider impact range within the model. This indicates that a larger portion of the stress generated by the explosive was exerted on the rocks, thereby resulting in a more effective stemming effect.

To study the stress propagation characteristics within the numerical model of rocks, monitoring points were strategically chosen. These points were located at a distance of 50 mm from the detonation center (H15360 element) and at a distance of 100 mm (H13140 element), as shown in Fig. 10. The stress conditions experienced by these monitoring points under different stemming conditions were analyzed.

By examining the stress-time curves at different monitoring points, it became evident that the shapes of the stress-time curves were similar across the three different stemming conditions. However, there are variations in the peak stress values generated during detonation. The highest peak stress value was observed when using the polyurethane foam material for stemming, followed by the clay material, while the non-stemmed blasting condition showed the lowest peak stress value. This observation suggests that stemming and detonation intensified the effect of explosive gases within the rock, resulting in a more focused impact from the detonation shock wave on the internal rock structure. Consequently, higher stress levels were experienced, facilitating the rock fragmentation. When comparing the stemming effects of polyurethane foam material and clay material, it became obvious that polyurethane foam material demonstrated superior stemming capabilities, as evidenced by the higher peak stress levels observed.

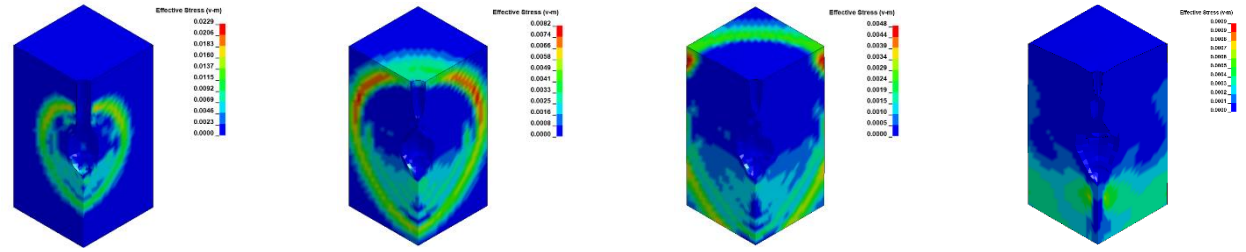

(a) No stemming

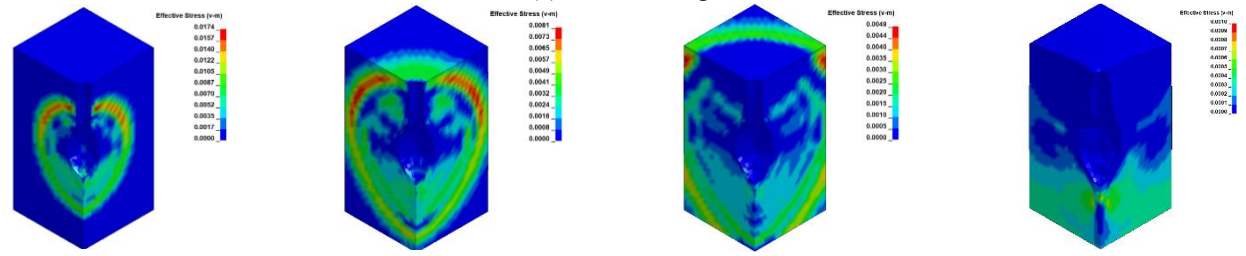

(b) Clay

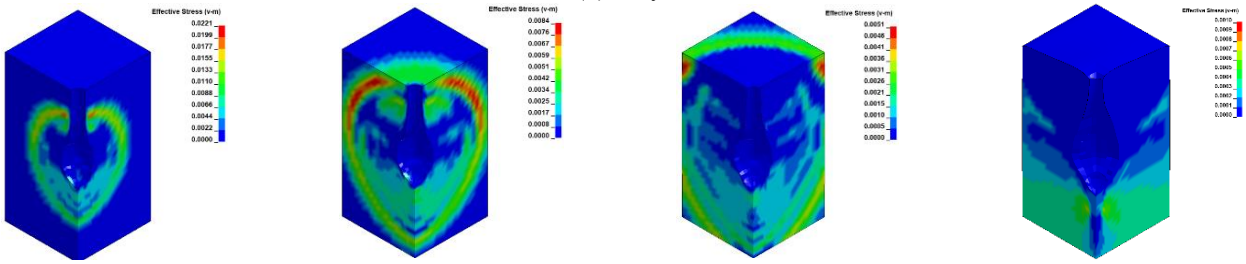

(c) Polyurethane

Fig. 9 Stress nephogram of rocks at different times after an explosion

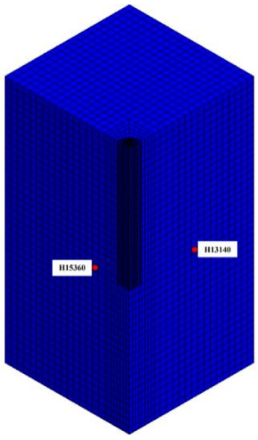

Fig. 10 Monitoring point locations

The comparison between the measured stress values from the blasting experiment and the numerical simulation results can be seen in Fig.12.

From Fig. 12, it is observed that the measured stress magnitudes from the blasting experiment exceeded the values obtained from numerical simulation calculation, which is because numerical simulations cannot fully consider all the influencing factors in reality. Moreover, the disparity became more obvious as the distance to the detonation center decreased, corresponding to a smaller scaled distance. This observation aligns with the information reported in the literature (Xin *et al*. 2019). However, despite the discrepancies, the numerical simulation results showed a satisfactory level of similarity with the blasting experiment. In terms of stress magnitude at different distances from the detonation center, it was observed that the highest stress levels were experienced when polyurethane foam material was used for stemming, followed by clay material, while the non-stemmed condition produced the lowest stress levels.

3.3.2 Model damage analysis

To explore the damage evolution in rocks under different stemming conditions, damage nephograms were extracted at different time intervals. To facilitate a

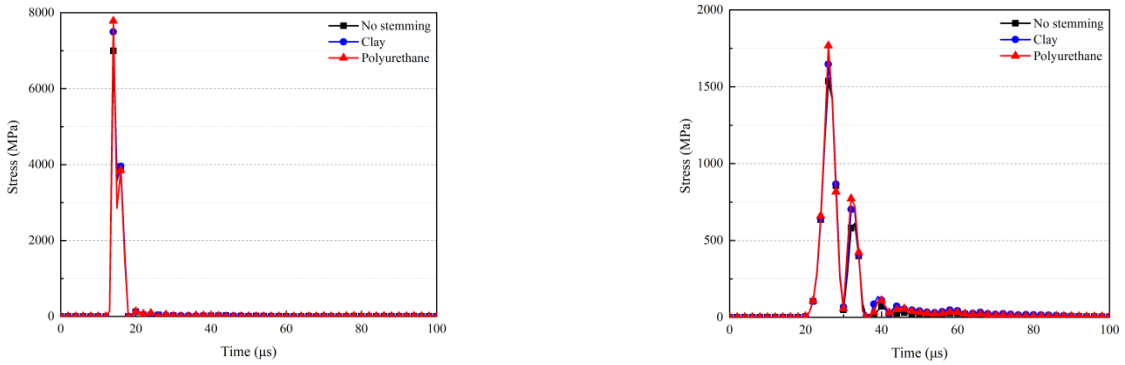

(a) 50 mm from the blast center (b) 100 mm from the blast center

Fig. 11 Stress-time curves at the monitoring points

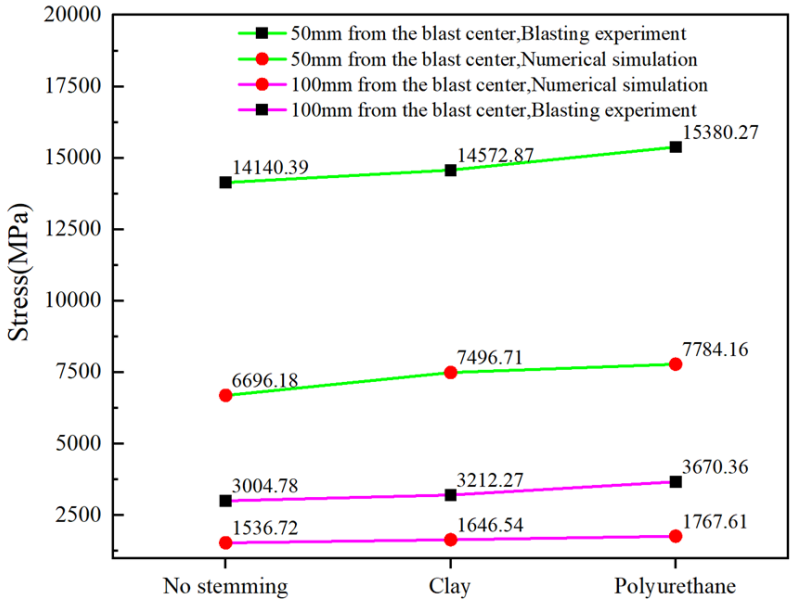

Fig. 12 Comparison of stress magnitudes

comprehensive observation of the internal damage in the rock, the 1/4 model was mapped to represent the entire rock mass for analysis and visualization. Fig. 13 presents the damage nephogram from left to right, corresponding to time intervals of 30 μs, 40 μs, 50 μs, and 100 μs, illustrating the progressive evolution of rock damage over time. Additionally, Fig. 12 shows the damage nephogram from left to right, representing time intervals of 30 μs, 40 μs, 50 μs, and 100 μs, showcasing the visual representation of the damage evolution in the rocks. To assess the extent of damage imposed on the rocks due to blasting, a damage factor denoted as D (Li *et al*. 2023b, He and Yang 2003) was used. The degree of fragmentation was described using this factor. When $D = 0$, it indicates that the rock remained undamaged. However, when $D > 0$, it signifies that the rock had experienced varying levels of damage. A value of $D = 1$ indicates complete fragmentation or total damage to the rock.

From the figure above, it is apparent that following the detonation of explosives, rocks under different stemming conditions experienced damage ($0 < D < 1$) or fragmentation ($D = 1$) primarily at the bottom of the blasthole due to the impact of the blast wave. The morphology patterns of rock damage under the three different stemming conditions showed general consistency. The instantaneous detonation at the bottom of the blasthole generated superimposed high-pressure stress waves, which rapidly fractured the rock under the influence of the detonation shock wave. Consequently, various-shaped cavities formed at the bottom of the blasthole. As the explosive action continued, these cavities progressively expanded and increased in volume.

At the early stage of 30 μs before the explosion, a damaged area emerged at the bottom of the blasthole in the rock. Subsequently, this damaged area gradually expanded. In the case of non-stemmed blasting, an "umbrella-shaped" damaged area formed in the lower part of the blasthole. However, due to the presence of stemming material, the detonation shock wave generated by the explosion reacted to propagate towards the sides of the blasthole. This resulted in the formation of a "funnel-shaped" damaged area at the bottom of the blasthole, with a narrower upper part and a wider lower part.

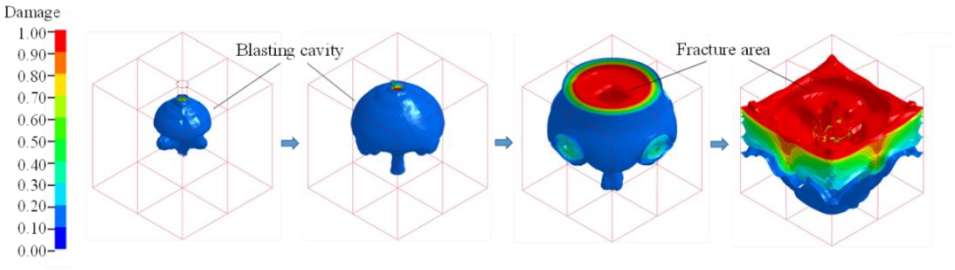

(a) No stemming

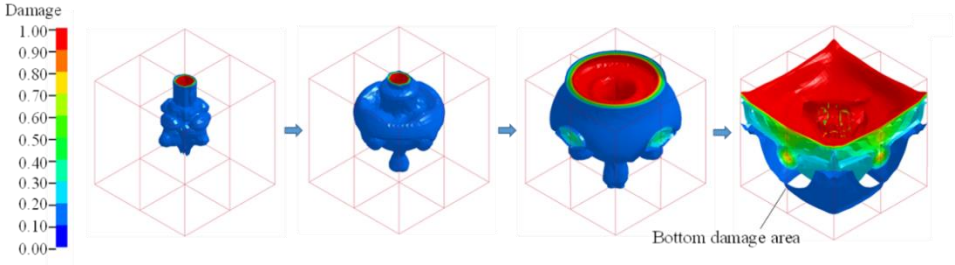

(b) Clay

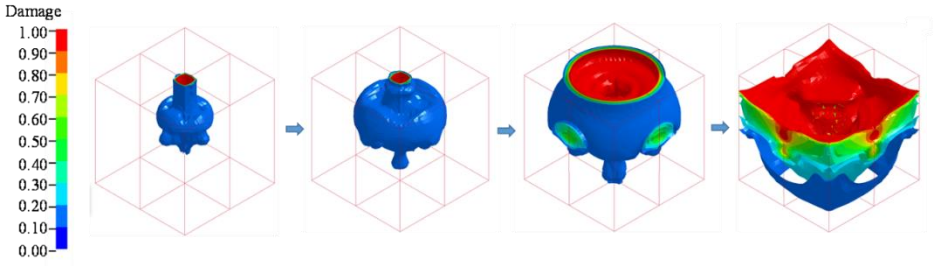

(c) Polyurethane

Fig.13 Damage nephogram at different time intervals

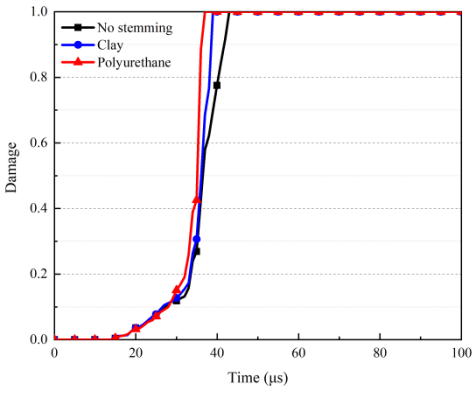

(a) 50 mm from the blast center

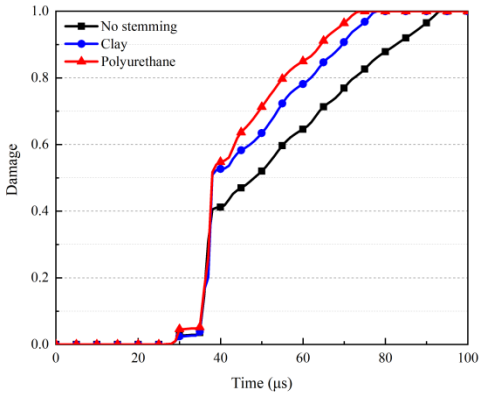

(b) 100 mm from the blast center

Fig. 14 Monitoring point damage time-history curves

Furthermore, the contour of the damaged area at the bottom of the blasthole, under the stemming effect of polyurethane foam material was larger compared to the clay material. As the explosion time increased, the damage area and destruction in the model gradually expanded. By 50 μs, the damaged area had essentially extended to the boundaries of the model. By 100 μs, the extent of damage and destruction in the model stabilized. In all three different stemming conditions, the rock models showed large cavities. In comparison to the non-stemmed condition, the cavities formed after the explosion under stemming conditions were larger. Moreover, the bottom of the model experienced a more extensive area of damage and destruction. The damage and fragmentation area following the explosion with polyurethane foam material as stemming was larger, indicating a more favorable stemming effect.

To study the variation of damage at different locations within the rock under different stemming conditions, two monitoring points, H15360 and H13140, were selected.

These points were located at distances of 50 mm and 100 mm from the blast center, respectively. The damage time-history curves obtained for these monitoring points under different stemming conditions are shown in Fig. 14.

From the graph, it is evident that at the monitoring point located 50 mm from the blast center, damage initiated after tens of microseconds from the initiation of the explosion.

Before reaching 40μs, all three different stemming conditions demonstrated significant levels of fragmentation at the monitoring point. At the monitoring point located 100mm from the blast center, damage began to occur around 40μs. As the explosion duration increased, the extent of damage at this monitoring point escalated to varying degrees under the three different stemming conditions. Comparatively, the damage observed during stemming conditions was considerably higher than that observed in the unstemmed condition. Furthermore, the time at which the monitoring point reached fragmentation (D=1) was earlier in the stemming condition than in the unstemmed condition. This disparity arose because stemming intensified the effect of stress waves generated by the explosion within the interior of the rock. The monitoring point experienced higher levels of stress during stemming, leading to increased damage compared to the unstemmed condition. Additionally, the time at which the monitoring point reached fragmentation occurred earlier during stemming. The higher level of damage observed at the monitoring point during stemming, particularly occurred when using polyurethane foam as the stemming material compared to clay, indicating the more effective stemming effect of polyurethane foam.

4. Discussion

4.1 The necessity of stemming

Based on the results of the blasting experiment, it was evident that the application of stemming to the blastholes led to higher internal blasting stress within the rock and resulted in smaller fragmentation of the rock mass. The numerical simulation results were consistent with the blasting experimental results, further confirming that when stemming was used in the blastholes, the fragmentation extent following the explosion was wider, the level of damage to the model was higher, and the time required for the rock to undergo damage and reach fragmentation is shorter.

During the explosion of the explosive, high-temperature and high-pressure gases rapidly exerted pressure on the specimen. In the absence of stemming, the explosive gases escaped from the blasthole, resulting in a decrease in internal pressure and a loss of energy during the explosion, reducing the destructive effect on the test specimen. However, when there was stemming in the blasthole, the stemming material prolonged the effective action time of the explosive gases on the test specimen, allowing a better utilization of energy for rock fragmentation. Stemming increased the effective stress of the explosive shock wave on rock breaking, making the rock more susceptible to crushing and damage, thereby reducing the occurrence of large intact rock masses. Consequently, stemming in blastholes was essential during blasting operations.

4.2 The mechanism of stemming

Following the explosion of the explosives, axial stress waves were generated in the blasthole, exerting pressure on both the surrounding rock and the stemming materials. In accordance with the laws of momentum and energy conservation, the stemming material experienced two main processes of motion within the blasthole. The first stage involved microscopic motion, whereby the blast-induced gases compressed the stemming material, leading to lateral expansion. Due to the radial confinement imposed by the blasthole, when the pressure wave reached the blasthole opening, the stemming materials started moving. The second stage involved macroscopic motion, where the outward expansion force (P) exerted by the blast-induced gases surpassed the self-weight of the stemming material and the frictional force (F) between the stemming material and the blasthole wall. Consequently, the stemming material collectively moved outward until it was expelled from the blasthole (Zong 1996, Luo and Shen 2006).

In practical terms, the self-weight of the stemming material was relatively small compared to the frictional resistance between the stemming material and the blasthole wall. Therefore, it was neglected in the analysis. Consequently, when examining the forces acting on the stemming material during the explosion, it was obvious that, under consistent blasting parameters and stemming length, the sealing effect primarily relied on the frictional resistance generated as the stemming material moved within the blasthole under the impact. This frictional resistance was influenced by the properties of the stemming material itself and the roughness of the blasthole wall. Therefore, it was closely associated with the frictional properties of the stemming material and the roughness of the blasthole wall.

Based on the data presented in Figure 2, the frictional force ranking for different stemming materials is as follows: Steel Mold > Plastic Mold ≈ Polyurethane Foam > Clay. Moreover, when considering the effectiveness of the stemming materials, the ranking is as follows: Polyurethane Foam ≈ Hollow Steel Mold ≈ Plastic Mold > Clay. This suggests that the effectiveness of stemming materials was influenced by both the frictional force and the sealing capability between the stemming materials and the blasthole wall.

- Clay material was considered as a loose type of stemming material, which generated less frictional resistance with the blasthole wall. When explosives detonated, it led to the phenomenon of blasthole punching (as shown in Fig. 15(a)). Although provided complete stemming of the blasthole, its stemming effectiveness was relatively poor compared to other stemming materials.
- Both the steel mold and plastic mold had a higher frictional force; however, due to the necessity of a channel for the detonator wires, they were not entirely sealed during stemming. As a result, during detonation, some high-pressure gas escaped through the gaps between the mold and the blasthole wall, leading to energy dissipation (as

shown in Figure 15(b, c)). This partially reduced the effectiveness of stemming to some extent, and their usage entails certain safety hazards.

• Although polyurethane foam material did not possess the highest frictional force, its exceptional sealing properties allowed the explosive gases to act more effectively on the rock, resulting in a more comprehensive rock fragmentation. Consequently, polyurethane foam material demonstrated a better stemming effectiveness.

In conclusion, polyurethane foam material for stemming offered several advantages: it exhibited strong adhesion to the blasthole wall, generating significant bonding strength and providing substantial frictional resistance. The foam's expansion and solidification created a complete seal within the blasthole, ensuring more effective confinement of the explosive gases, minimizing their escape, and allowing them to exert a greater effect on the rock. Additionally, the self-expanding properties of the polyurethane foam mixture made it easier to place at the blasthole opening, simplifying the operation. Overall, polyurethane foam material exhibited great potential for practical applications in engineering projects.

5. Conclusions

In this study, an analysis and comparison of the blasting effect on rock breaking under different stemming conditions were conducted, along with a study on the mechanism of stemming. Based on the results obtained from the blasting experiment under different stemming conditions, several observations can be made. The presence of stemming led to greater internal blasting stress within the rock, and the blasting stress decreased significantly with an increasing distance from the blasting center. Moreover, the use of stemming materials resulted in smaller rock fragmentation. Among the different types of stemming materials examined, polyurethane foam, steel mold, and plastic mold exhibited better stemming effects, with a majority of the post-blasting rock fragments being below 50 mm in size. On the other hand, the stemming effect of clay was comparatively less effective (poor).

The numerical simulation results correlated well with the conclusions drawn from the blasting experiment. When stemming was implemented, the range of rock affected by the blasting stress wave was wider, and the overall stress exerted on the rock increased. Similarly, as the distance from the blasting center increased, the magnitude of internal blasting stress within the rock decreased significantly. The presence of stemming led to elevated levels of rock damage, earlier fragmentation, and a larger area of fragmentation. The numerical simulation results validated the superior stemming effect of polyurethane foam material compared to clay material.

The sealing performance of the stemming materials was closely linked to their generated frictional resistance and sealing capability. Polyurethane foam material exhibited strong adherence to the blasthole walls, creating a strong bond and providing significant frictional resistance. This ensured a complete stemming state, effectively reducing the escape of explosive gases and maximizing their impact on the rock. Furthermore, the use of polyurethane foam material was relatively simple and easy, making it a promising option for engineering applications.

References

Brinkmann, J.R. (1990), "An experimental study of the effects of shock and gas penetration in blasting", *Proceedings of the 3rd International Symposium on Rock Fragmentation by Blasting*, Brisbane, Australia, August.

Cevizci, H. and Ozkahraman, H.T. (2012), "The effect of blast hole stemming length to rockpile fragmentation at limestone quarries", *Int. J. Rock Mech. Min.*, **53**, 32-35. https://doi.org/10.1016/j.ijrmms.2012.04.005.

Chen, M., Ye, Z.W., Lu, W.B., Wei, D. and Yan, P. (2021a), "Corrigendum to An improved method for calculating the peak explosion pressure on the borehole wall in decoupling charge blasting", *Int. J. Impact Eng.*, **156**, 103945. https://doi.org/10.1016/j.ijimpeng.2021.103945.

Chen, M., Ye, Z.W., Wei, D., Lu, W.B. and Yan, P. (2021b), "The movement process and length optimization of deep-hole blasting stemming structure", *Int. J. Rock Mech. Min.*, **146**, 104836. https://doi.org/10.1016/j.ijrmms.2021.104836.

Choudhary, B.S. and Rai, P. (2013), "Stemming plug and its effect on fragmentation and muckpile shape parameters", *Int. J. Min. Min. Eng.*, **4**(4), 296-311. https://doi.org/10.1504/ijmme.2013.056854.

Dally, J.W., Fourney, W.L. and Holloway, D.C. (1975), "Influence of containment of the bore hole pressures on explosive induced fracture", *Int. J. Rock Mech. Min. Sci. Geomech. Abstracts*, Pergamon, January.

Fourney, W.L., Barker, D.B. and Holloway, D.C. (1981), "Model studies of explosive well stimulation techniques", *Int. J. Rock Mech. Min. Sci. Geomech. Abstracts*, Pergamon, April.

He, C.L. and Yang, J. (2019), "Experimental and numerical investigations of dynamic failure process in rock under blast loading", *Tunn. Undergr. Sp. Tech.*, **83**, 552-564, https://doi.org/10.1016/j.tust.2018.08.047.

José, A.S., Segarra, P. and López, L.M. (2007), "Energy components in rock blasting", *Int. J. Rock Mech. Min.*, **44**(1), 130-147. https://doi.org/10.1016/j.ijrmms.2006.05.002.

Kojovic, T. (2005), "Influence of aggregate stemming in blasting on the SAG mill performance", *Miner. Eng.*, **18**(15), 1398-1404. https://doi.org/10.1016/j.mineng.2005.02.012.

Konya, C.J. and Walter, E.J. (2003), *Rock Blasting and Overbreak Control*, (2nd Ed.), V.A. National Highway Institute, Arlington, VA, USA.

Lee, K., Kim, T. and Kim, J. (2009), "Local response of W-shaped steel columns under blast loading", *Struct. Eng. Mech.*, **31**(1), 25-38. https://doi.org/10.12989/sem.2009.31.1.025.

Li, C.R., Kang, L.J., Qi, Q.X., Mao, D.B., Liu, Q.M. and Xu, G. (2009), "The numerical analysis of borehole blasting and application in coal mine roof-weaken", *Procedia Earth Planet Sci.*, **1**(1), 451-459. https://doi.org/10.1016/j.proeps.2009.09.072.

Li, F., Liu, H.W., Xiang, G.Y., Ren, B.R., Zou, Y.L. and Sun, R.C. (2023a), "The numerical simulation of rapid excavation technologies under the combined form of hydraulic fracturing and drill-and-blast method", *J. Build. Eng.*, **73**, 106757. https://doi.org/10.1016/j.jobe.2023.106757.

Li, X.D., Liu, K.W., Sha, Y.Y., Yang, J.C. and Song, R.T. (2023b), "Numerical investigation on rock fragmentation under decoupled charge blasting", *Comput. Geotech.*, **157**, 105312. https://doi.org/10.1016/j.compgeo.2023.105312.

Liu, B.B., Ji, R.C. and Lu, S.X. (2021), "Numerical simulation of

underwater drilling and blasting based on ANSYS/LS-DYNA", *Sci. Technol. Eng.*, **21**(27), 11776-11782. (in Chinese)

Liu, B. and Huang D. (2015), "Water stemming application on large-diameter longhole blasting", *Nonferr. Met. Eng.*, **5**(Z1), 116-119. (in Chinese)

LSTC (2003), LS-DYNA Keyword User's Manual, Livermore Software Technology Corporation, Livermore, CA, USA.

Luo, Y. and Shen Z.W. (2006), "Study on length of stemming material and its effect in hole-charged blasting", *Mech. Pract.*, **28**(2), 48-52. (in Chinese)

Ma, C.D., Liu Z.L. and Wang, Y.S. (2020), "A new method for rapid blockage of boreholes in large-section tunneling excavation", *Min. Metall. Eng.*, **40**(4), 6-9. (in Chinese)

Mackerle, J. (1999), "Finite element and boundary element technology in rock and mining mechanics A bibliography (1995–1998)", *Finite Elem. Anal. Des.*, **31**(4), 317-325. https://doi.org/10.1016/s0168-874x(98)00066-3.

Onder, U., Ercan, A. and Mehmet, B. (2007), "Studies on the effect of burden width on blast-induced vibration in open-pit mines", *Environ. Geol.*, **53**(3), 643-650. https://doi.org/10.1007/s00254-007-0679-9.

Otuonye, F.O., Konya, C.J. and Skidmore, D.R. (1983), "Effects of stemming size distribution on explosive charge confinement: A laboratory study", *Min. Eng.*, **35**(8), 1205-1208.

Sazid, M.D., Saharan, M.R. and Singh, T.N. (2011), "Effective explosive energy utilization for engineering blasting–initial results of an inventive stemming plug", *Proceedings of the 12th ISRM International Congress on Rock Mechanics*, Beijing, China , October.

Tu, Z.G. and Lu, Y. (2010), "Modifications of RHT material model for improved numerical simulation of dynamic response of concrete", *Int. J. Impact Eng.*, **37**(10), 1072-1082. https://doi.org/10.1016/j.ijimpeng.2010.04.004.

Wang, H.C., Wang, Z.L., Wang, J.G., Wang, S.M., Wang, H.R., Yin, Y.G. and Fang,L. (2021a), "Effect of confining pressure on damage accumulation of rock under repeated blast loading", *Int. J. Impact Eng.*, **156**, 103961. https://doi.org/10.1016/j.ijimpeng.2021.103961.

Wang, S., Feng, H.Y., Hong, J.M. and Wang, G.L. (2023), "Enhanced foaming ability of thermoplastic polyurethane by crystallization during mold-opening foam injection molding with supercritical N2 as blowing agents", *J. Mater. Res. Technol.*, **22**, 2489-2501. https://doi.org/10.1016/j.jmrt.2022.12.117.

Wang, Z.L., Wang, H.C., Wang, J.G. and Tian, N.C. (2021b), "Finite element analyses of constitutive models performance in the simulation of blast-induced rock cracks", *Comput. Geotech.*, **135**, 104172. https://doi.org/10.1016/j.compgeo.2021.104172.

Xie, C.Y., Nguyen, H., Bui, X.N., Choi, Y., Zhou, J. and Thao, N.T. (2021), "Predicting rock size distribution in mine blasting using various novel soft computing models based on meta-heuristics and machine learning algorithms", *Geosci. Front.*, **12**(3), 101108. https://doi.org/10.1016/j.gsf.2020.11.005.

Xin, C.L., Tu, J., Wang, J.L., Sun, F.T. and Liu, A.Y. (2019), Master LS-DYNA from easy to deep, Water Conservancy and Hydropower Publishing Press, Bei Jing, China.

Xu, M.Q., Luo, H.Y., Rong, H.W., Wu, S.H., Zheng, Z.X. and Chen, B.Y. (2023), "Calcium alginate gels-functionalized polyurethane foam decorated with silver nanoparticles as an antibacterial agent for point-of-use water disinfection", *Int. J. Biol. Macromol.*, **231**, 123289. https://doi.org/10.1016/j.ijbiomac.2023.123289.

Xu, S.L., Wu, P., Li, Q.H., Zhou, F. and Chen, B.K. (2021), "Experimental investigation and numerical simulation on the blast resistance of reactive powder concrete subjected to blast by embedded explosive", *Cement Concrete Comp.*, **119**, 103989. https://doi.org/10.1016/j.cemconcomp.2021.103989.

Yan, C.L. and Shi, Z.Q. (2014), "Study on tunnel blasting technology of Ste Holes by water-clay composite", *Sci. Technol. Eng.*, **14**(26), 300-303. (in Chinese)

Yuan, Y., Lan, Q.G., Ding, L., Yang, H.G., Gao, H.B., Wang, Z.Y., Yang, C.J. and Deng, Z.Q. (2022), "Estimation of interaction forces with minimal parameters for rigid wheels on deformable terrain using modified Hooke's law", *Mech.. Mach. Theory*, **169**, 104663. https://doi.org/10.1016/j.mechmachtheory.2021.104663.

Zhang, Z.X., Hou, D.F., Guo, Z. and He, Z. (2020), "Laboratory experiment of stemming impact on rock fragmentation by a high explosive", *Tunn. Undergr. Sp. Tech.*, **97**, 103257. https://doi.org/10.1016/j.tust.2019.103257.

Zhang, Z.X., Qiao, Y., Chi, L.Y. and Hou, D.F. (2021), "Experimental study of rock fragmentation under different stemming conditions in model blasting", *Int. J. Rock Mech. Min.*, **143**, 104797. https://doi.org/10.1016/j.ijrmms.2021.104797.

Zong, Q. (1996), "Theoretical discussion on movement law of borehole blockage", *Blasting*, **1**, 8-11. (in Chinese)

CC